Comparison of the flexural behavior of natural and thermo-hydro-mechanically densified Moso bamboo

Citation: Dixon, P. G. et al. "Comparison of the Flexural Behavior of Natural and Thermo-Hydro-Mechanically Densified Moso Bamboo." European Journal of Wood and Wood Products 74.5 (2016): 633–642.

As Published: http://dx.doi.org/10.1007/s00107-016-1047-9

Publisher: Springer Berlin Heidelberg

Persistent URL: http://hdl.handle.net/1721.1/106660

Version: Author's final manuscript: final author's manuscript post peer review, without publisher's formatting or copy editing

Comparison of the flexural behavior of natural and thermo-hydro-mechanically densified Moso bamboo

Dixon PG[1], Semple KE[2], Kutnar A[3], Kamke FA[4], Smith GD[2], Gibson LJ[1,*]

[1]Department of Materials Science and Engineering, Massachusetts Institute of Technology
77 Massachusetts Ave, Cambridge, MA 02139, USA

[2]Department of Wood Science, University of British Columbia
#2900- 2424 Main Mall, Vancouver, BC, Canada V6T 1Z4

[3]Andrej Marušič Institute, University of Primorska
Muzejski trg 2, 6000 Koper, Slovenia

[4]Department of Wood Science and Engineering, Oregon State University
119 Richardson Hall, Corvallis, OR 97331, USA

*Corresponding author at: Massachusetts Institute of Technology, 77 Massachusetts Ave, Bldg. 8-135, Cambridge, MA 02139, USA. E-mail address: ljgibson@mit.edu (L.J. Gibson).

Abstract

The flexural properties in the longitudinal direction for natural and thermo-hydro-mechanically densified Moso bamboo (*Phyllostachys pubescens* Mazel) culm wall material are measured. The modulus of elasticity (MOE) and modulus of rupture (MOR) increase with densification, but at the same density, the natural material is stiffer and stronger than the densified material. This observation is primarily attributed to bamboo's heterogeneous structure and the role of the parenchyma in densification. The MOE and MOR of both the natural and densified bamboo appear linearly related to density. Simple models are developed to predict the flexural properties of natural bamboo. The structure of the densified bamboo is modelled, assuming no densification of bamboo fibers, and the flexural properties of densified bamboo are then predicted using this structure and the same cell wall properties of that of the natural material modelling. The results are then compared with those for two analogous structural bamboo products: Moso bamboo glulam and scrimber.

Introduction

Bamboo is an under-utilized material that could be used more efficiently in structural bamboo products (SBP), engineered products analogous to glue-laminated wood, oriented strand board and plywood. About 30 million hectares of bamboo resources are distributed worldwide and the plant's fast growth make it competitive with wood in terms of biomass yield (Jiang 2007; FAO 2010; Vogtländer et al. 2010). Improved fundamental understanding of the structure and mechanical properties of bamboo, and of bamboo processing, could foster the adoption of structural bamboo products, extending the use of bamboo.

Bamboo has a more heterogeneous structure than wood. Bamboo has a fiber-reinforced composite-like structure, consisting of vascular bundles, relatively large arrangements of dense sclerenchyma fibers supporting vessels, in a matrix of lower density parenchyma (Liese 1987). The fiber volume fraction increases radially from the inside to the outside of the culm wall and longitudinally, up the height of the culm (Grosser and Liese 1971; Liese 1987; Amada et al. 1997; Lo et al. 2004; Shao et al. 2010).

Two important structural bamboo products are glue-laminated bamboo (glulam) and scrimber (Jiang 2007; Ramage et al. 2015). Conventional wood glulam is made by gluing together long strips of wood to make up large members (Lam 2001; Forest Products Laboratory 2010). Glulam appears to be an ideal application for bamboo; however, this product has a low material use efficiency, with only roughly 30% of the culm inputs being used in the product (Lugt 2008). Bamboo scrimber, also known as strand woven bamboo, is a highly dense product consisting of crushed sections of bamboo culms, covered with resin, compressed and heated; it has a material use efficiency of about 80%, higher than that of bamboo glulam (Lugt 2008; Yu et al. 2015; Ramage et al. 2015). Bamboo oriented strand board (OSB) is an additional product, which to an extent combines the mechanical efficiency (specific stiffness and specific strength)

of the natural bamboo tissue with high material use efficiency (Semple et al. 2015b). While there have been several studies regarding bamboo OSB fabrication and properties (Lee et al. 1996; Sumardi et al. 2007, 2015; Semple et al. 2015b, c, d), bamboo OSB has yet to be fully commercialized (Semple et al. 2015c,b).

For many composite wood products, an important aspect of their processing is densification, which occurs as a secondary effect during the hot-pressing operation needed for thermosetting adhesives (Kamke and Casey 1988; Wolcott et al. 1994; Winistorfer et al. 2000). Densified wood as a product in itself has potential to be a useful material. Thermo-hydro-mechanical (THM) compression processes on wood, combining steam and compression at elevated temperature, can produce material with higher mechanical properties than natural wood (Kamke 2006; Kutnar et al. 2008, 2009). One such process is known as viscoelastic thermal compression (VTC), which is a type of THM process (Kamke and Sizemore 2008). The effect of the heat in VTC is to bring the wood cell wall above its glass transition temperature, which has been reduced by plasticization from steam. The compression of the wood then buckles the softened cell walls without fracturing them, resulting in a wood density increase with corresponding stiffness and strength increases (Kamke 2006; Kutnar et al. 2008, 2009; Kamke and Rathi 2011).

Similarly, densification could be important for processing structural bamboo products; it is certainly involved in processing scrimber and could be in other bamboo products. Due to the more heterogeneous structure of bamboo, compared with wood, bamboo will densify differently, and the properties of bamboo may be altered in a way unlike that of wood. Initial direct investigations of the fabrication and properties of THM densified bamboo products have recently been carried out (Semple et al. 2013, 2015a; Archila-Santos et al. 2014). The longitudinal

Young's moduli of densified Guadua (*Guadua angustifolia* Kunth) materials increase as a result of densification, giving an increase in specific stiffness from 0.030 GPa m^3/kg at a density of 540 kg/m^3 to 0.038 GPa m^3/ kg at a density of 830 kg/m^3 (Archila-Santos et al. 2014). The flexural modulus of elasticity (MOE) and the modulus of rupture (MOR) along the longitudinal direction of Moso (*Phyllostachys pubescens* Mazel) materials, densified using the VTC closed-chamber steam press, both increase compared with undensified material (Semple et al. 2013). However, from exploratory trials on THM densification of Moso bamboo material, densified bamboo appears to have a lower MOE than that of natural Moso bamboo material of similar high density, from the outer regions of the culm wall (Semple et al. 2013).

In this study, the flexural properties along the longitudinal direction of natural and THM densified Moso bamboo are measured. Rule of mixture models are developed to estimate the density, the MOE, and the MOR of natural Moso bamboo. A simple model of bamboo densification is developed to abstract the structural changes in the tissue resulting from densification. The model for the densified structure is then used, along with rule of mixtures, to estimate the MOE and MOR of densified bamboo. Finally, the flexural properties of Moso bamboo glulam and scrimber, available in the literature, are compared with those of the natural and THM densified Moso bamboo material.

Materials and Methods

Materials

The materials used are from a lower section of a Moso culm, obtained from the importer Bamboo Craftsman Company (Portland, Oregon). Prior to importation, the culm underwent a borate treatment, as is required for importation from China to the United States. In this paper,

materials cut directly from the culm section without densification are simply referred to as "natural." Age of the imported culm materials is noted as 3 to 6 years by the importer.

Densification

Tangentially and radially oriented strips were cut from the Moso culm section (**Fig. 1**). The strips were subsequently sanded so that each strip was of uniform thickness, between 3 and 5 mm. Nominal strip length and width were 90 and 20 mm, respectively. The tangential strips were cut from the inner regions of the culm wall, i.e. the lower density regions. Strips of clear internode material and strips with nodes near their midpoints were prepared for both orientations. Approximately half of the strips (roughly 40) were compressed to 50% of their original thickness in a VTC process, using the same densification procedure as that of Semple et al. (2013). In a previous study, Semple et al. (2013) found that compression to 50% (1080 kg/m^3 average density) was optimal for void-space closure whereas compression to 33% thickness (1261 kg/m^3 average density) caused excessive lateral displacement and shear damage to the tissue. The VTC process was a closed chamber procedure with platen temperatures of 170˚C. Maximum steam pressure during the process was 775 kPa; exposure to pressurized steam was about 150 s. Total processing time was roughly 800 s. Note the strips were densified along their thicknesses, meaning the radially oriented strips were densified along the tangential direction and tangentially oriented strips were densified along the radial direction. The remaining natural strips were further sanded in their natural state to more closely match the thickness of the densified specimens.

Imaging

Cross-sections (normal to the longitudinal direction) of specimens were imaged with a JEOL JSM-6610LV scanning electron microscope (Peabody, MA). Surfaces were prepared by

grinding on a Struers Rotopol-1 model polishing wheel (Cleveland, OH) with progressively finer silicon carbide papers: 800-grit, 1200-grit, 2400-grit, and 4000-grit. After air-drying, samples were imaged. Most specimens used for imaging were uncoated and imaged in low vacuum mode, at roughly 30 Pa.

Bending

Two flexural test specimens (termed 'beams') were laser cut from roughly 25 individual strips for each case (natural and densified). This procedure created inner and outer bending test specimens from each radial strip (width along the radial direction), while for tangential strips it simply created a duplicate (width along the tangential direction); beam locations are shown on the strips in **Fig. 1**. Beam dimensions were as follows: width 5 mm, depth 1-3 mm and length 70 mm. Dimensions and masses of all the beams were measured at their respective moisture contents and used to calculate specimen density. Three-point bending was performed using a span of 60 mm. The beams were tested in an Instron model 4201 (Norwood, MA) at a speed of 2 mm/min. The central deflection was measured with a linear variable differential transducer (Trans-Tek 240 Series; Ellington, CT) and the load was measured with a 500 N load cell. A total of 44 densified and 42 natural specimens were tested. Specimens were not specifically selected or grouped by density; the determined density of each beam was simply linked to its respective obtained MOE and MOR.

Moisture Content

Six natural and six densified beams post-testing were used to determine the moisture content gravimetrically. The specimens were put in an oven at 103˚C for 24 h and the moisture content was calculated from the air-dry and oven-dry weights.

Nanoindentation

Tangentially cut natural and densified sections were mounted in epoxy (one each) at atmospheric pressure. The cross-sections were perpendicular to the indentation axis. Surfaces were prepared by the same method as noted for microscopy. Nanoindentation was performed with a Hysitron TriboIndenter (Minneapolis, MN), equipped with a Berkovich tip and a dynamic mechanical analysis transducer. A maximum load of 500 μN was used. Each sample received 96 indents on the fiber areas. Atypically shaped load-depth curves were removed from analysis leaving 94 and 88 indents in the natural and densified cases, respectively.

Modelling

Natural bamboo can be modelled using a simple rule of mixtures approach. The tissue can be considered composed of two constituents, fibers (referring to actual sclerenchyma fibers, opposed to vascular bundles) and parenchyma. This assumes other constituents (vessels, sieve tubes, and the additional cells of the vascular bundle, some of which are parenchyma (Grosser and Liese 1971)) are treated the same as the basic parenchyma surrounding the vascular bundles. Vessels and sieve tubes compose roughly 10% of the culm tissue (Liese 1987) and calculations using the vascular bundle volume fraction and solid fraction suggest a combined vessel (vessels and sieve tubes) volume fraction from 3 to 6% (Dixon and Gibson 2014). The density, ρ^* of such a structure is then given by the rule of mixtures:

$$\rho^* = \rho_f V_f + \rho_p^* V_p \quad (1)$$

where ρ is the density, V is the volume fraction, the subscripts f and p refer to fibers and parenchyma, respectively, and with $V_p = 1 - V_f$. As the sclerenchyma fibers have an extremely small lumen, in the tissue studied, they are assumed to have the same density, ρ_f (fiber density), as the solid cell wall in wood, ρ_s (wood solid cell wall density), $\rho_f = \rho_s = 1500$ kg/m^3 (Gibson

and Ashby 1997). The density of the parenchyma can be estimated from the measured relative density $\left(\rho_p^* / \rho_s\right)_p = 0.22$ available in the literature; assuming the same solid cell wall density, then the density of the parenchyma is ρ_p^* = 330 kg/m^3 (Dixon and Gibson 2014). As noted above, this density is that of the parenchyma surrounding the vascular bundles and is applied to the volume that is not fiber.

The longitudinal Young's modulus of the bamboo, E^*, which the longitudinal MOE approximates, is given by the same rule of mixtures:

$$E^* = E_f V_f \tag{2}$$

where E_f is the Young's modulus of the sclerenchyma fibers. The MOE underestimates the Young's modulus by roughly 1-5%, given the span to depth ratios used, assuming similar ratios of elastic constants to wood (Bodig and Jayne 1982); for the remainder of the paper they were taken to be the same. Here, the parenchyma contribution to the longitudinal Young's modulus is neglected ($E_p \sim 0$), as the fibers dominate the mechanical response even at low fiber volume fraction: in a previous study, the fiber contribution was found to account for roughly 90% of the measured longitudinal MOE in Moso bamboo even at low fiber volume fraction and density (Dixon and Gibson 2014). The longitudinal Young's modulus of the fiber, E_f, can be estimated using the extrapolated value of 39.8 GPa, available in the literature (Dixon and Gibson 2014).

This rule of mixtures can be extended to the longitudinal MOR, albeit non-rigorously:

$$MOR^* = MOR_f V_f \tag{3}$$

using a MOR_f of 472 MPa from literature (Dixon and Gibson 2014). The parenchyma contribution has similarly been neglected; in the previous study, the fiber contribution was found

to account for roughly 85% of measured longitudinal MOR at low fiber volume fraction and density (Dixon and Gibson 2014).

If the fiber volume fraction is assumed to vary from 0.05 to 0.50, a range indicative of the variation across the bamboo culm wall (Amada et al. 1997; Shao et al. 2010; Liu et al. 2014; Dixon and Gibson 2014), paired (i.e. at the same fiber volume fraction) densities, longitudinal Young's moduli, longitudinal MORs can be calculated.

Additionally, densification can be modelled to approximate the densified bamboo structure and properties. The following simple treatment of the densification applies only up to an initial fiber volume fraction of the natural material of approximately 0.36. The fiber volume fraction of natural specimens in this study ranged from roughly 0.10 to 0.23, calculated based on their density with Eq. 1, well within this limit. During densification, the thickness, t of a specimen is reduced to a fraction, C, of the original thickness; in this study C is 0.5.

$$t_{dens} = Ct \tag{4}$$

If lateral expansion is ignored, the original specimen width and length, b and l, are the same as the final specimen width and length. The plastic Poisson's ratio of cellular solids is typically close to zero (Shaw and Sata 1966), and THM compression to 50% of the thickness in Moso bamboo with the same VTC device is noted to cause only slight lateral expansion (Semple et al. 2013). It is noted that Eq. (4) could be modified to include the width, and C could be adjusted to account for lateral expansion, if a value of the plastic Poisson's ratio was considered.

The fibers are virtually solid in the tissue studied, thus their total volume cannot change during plastic deformation. The new fiber volume fraction, after densification, then becomes

$$V_{f_{dens}} = V_f / C \tag{5}$$

In this particular case, with C = 0.5, the fiber volume fraction doubles. This expression is based on the assumption of fully solid fibers and neglects natural variability in the ratio of cell wall thickness to cell diameter. In immature bamboo tissue (or any bamboo tissue otherwise with fibers that have significant lumen relative to cell wall thickness) (Liese and Weiner 1996; Gritsch 2004), this assumption cannot be made. The new parenchyma volume fraction is simply given by

$$V_{p_{dens}} = 1 - V_{f_{dens}} \tag{6}$$

The parenchyma tissues densifies, i.e. the relative density increases. The total volume of parenchyma solid cell wall is given as the product $bltV_p\left(\rho_p^* / \rho_s\right)_p$. The total volume of parenchyma tissue in the densified structure is given by $CbltV_{p_{dens}}$. The new relative density is then given by the quotient:

$$\left(\rho_{p_{dens}}^* / \rho_s\right)_{p_{dens}} = \frac{\left(\rho_p^* / \rho_s\right)_p V_p}{CV_{p_{dens}}} \tag{7}$$

The properties now can be modeled using the new fiber and parenchyma volume fractions and the new parenchyma relative density. The equations are as follows

$$\rho_{dens}^* = \rho_f V_{f_{dens}} + \rho_s \left(\rho_{p_{dens}}^* / \rho_s\right)_{p_{dens}} V_{p_{dens}} \tag{8}$$

$$E_{dens}^* = E_f V_{f_{dens}} \tag{9}$$

$$MOR_{dens}^* = MOR_f V_{f_{dens}} \tag{10}$$

with the fiber and parenchyma solid cell wall properties unchanged. The parenchyma contribution to the MOR is neglected, as is the case with E.

Results and Discussion

Densification of the parenchyma and closure of the vessels are evident from the micrographs in **Fig. 2**. The parenchyma have undergone large plastic deformations without

noticeable fracture of the cell walls, similar to wood processed by VTC (Kamke 2006; Kutnar et al. 2009). The highly dense fibers appear undeformed.

The longitudinal MOE and MOR of the natural and densified bamboo are plotted with respect to density in **Fig. 3**. The data for natural bamboo from this study match those of the previous study (Dixon and Gibson 2014), albeit over a lower range of densities, about 450 to 600 kg/m^3 (average ± standard deviation, 527 ± 44 kg/m^3); the specimens from the previous study were from tangential cuts at different radial positions, giving the larger range of densities. The moisture content of the natural specimens in this study was 7%. That of the previous study was 4% (Dixon and Gibson 2014; Dixon et al. 2015). The densified specimens' density ranges from 800 to 1200 kg/m^3 (average ± standard deviation, 997 ± 124 kg/m^3). The moisture content of the densified specimens was 5%. There was little difference between tangential and radial cut specimens, internode specimens and specimens containing a node; graphs showing the data by these individual groups are available in the supplemental information (**Online Resource 1**).

Overall, the natural and densified bending properties along the longitudinal direction vary linearly with density (**Fig. 3**), as would be expected given the fiber-reinforced composite-like structure of bamboo. Densification increases the bamboo's flexural properties, but the highest density natural material from this study is stiffer and stronger than the lowest density densified materials, even though this natural material is 25% less dense.

When the flexural properties of the densified bamboo are compared to those of the natural Moso material at the same density from an earlier study (Dixon and Gibson 2014), the relative reduction is even more apparent. The densest natural material from the previous study is about twice as stiff and strong as the densified material from this study, at the same density. This is an expected, though undesirable, result. The scatter in the densified material MOR is higher

than that of the natural material as might be expected due to damage in the microstructure as a result of the THM process.

The models are also plotted in **Fig. 3**, using the densities calculated from equations (1) and (8) at a given fiber volume fraction, paired with flexural properties calculated with equations (2, 3) (for the natural material) and (9, 10) (for the densified material) at the same fiber volume fraction. The models relating the MOE to density give a good description of the experimental results for both the natural and densified materials (**Fig. 3a**). The models capture the range and variation of MOE with density of the natural and densified material well, and, more importantly, capture the relative MOE reduction of the densified material. The contribution of the parenchyma to the MOE appears to be negligible, so that it is appropriate to neglect it.

The MOR-density model for the natural bamboo also describes the experimental data well (**Fig. 3b**). The MOR-density model for the densified bamboo generally underpredicts the experimental data (**Fig. 3b**), suggesting the densified parenchyma does have a meaningful contribution to the MOR, which appears to be a roughly constant 30 MPa at all densities. This result implies the densification of the parenchyma, the closure of the vessels, or possibly a combination of the two positively alters the weakest link and related failure mechanism in the bamboo structure. Despite the under-prediction, the model captures the general range of the MOR, the MOR's variation with density, and the relative MOR reduction of the densified material.

In general, the fibers have very small lumens and are nearly all cell wall substance in the natural Moso bamboo (**Fig. 2**); densification occurs by parenchyma densifying and vessels closing. Flexural properties along the longitudinal direction are likely dominated by the fibers' contribution, in the natural state of the bamboo material. Even in the case of densified

parenchyma (stiffer and likely stronger than the natural parenchyma material), the fibers' contribution likely still dominates, especially if damage to parenchyma as a result of densification is considered. Then, the purely geometrical increase in fiber volume fraction is the most substantial change affecting mechanical properties from the parenchyma densification. However, the increase in density of the bamboo tissue exceeds that of the fiber volume fraction, and the fiber volume fraction, MOE and MOR of the densified material are less than that of the equally dense natural material.

The densification model crudely simulates the densification of the parenchyma and increase in the fiber volume fraction, without fiber densification. The exclusion of the parenchyma contribution from the mechanical properties assumes the fibers' dominance. As mentioned previously, for the natural bamboo specimens in the current study, the density range was roughly 450 to 600 kg/m^3, which corresponds to a fiber volume fraction of roughly 0.10 to 0.23 (Eq. 1). Given the preparation method, namely tangential beams from the inner culm wall regions and radially oriented beams, the low fiber volume fraction is expected. Using the range 0.10 to 0.23 for the natural bamboo fiber volume fraction (corresponding to the natural bamboo density prior to densification), a density range for the densified bamboo from roughly 890 to 1200 kg/m^3 is calculated with the densification model, agreeing relatively well with the observed range.

The correspondence between the natural and densified density suggests the simple model of bamboo densification is appropriate. Likewise, the satisfactory agreement of MOE- and MOR- density models with experimental data imply appropriate modelling of the mechanical properties and structure. Thus, the densification of parenchyma, which produces a structure with lower volume fraction of fibers at a given density than the natural bamboo structure, is suggested

as the primary reason for the lower stiffness and strength of the densified bamboo compared to the high density natural bamboo. The THM compression study of Semple et al. (2013) found MOR and MOE increased proportionally with increasing compaction level and density (219 MPa and 13.6 GPa at the maximum compression to 33%), but also noted that the MOE in particular of the THM densified bamboo is lower than values for the outer wall of natural bamboo. Flattening of the cross-sectional profiles of the reinforcing fiber bundles was observed during compression changing their shape from longer in the radial direction to longer in the tangential direction (in tangential strips, densified along the radial direction) (Semple et al. 2013). This was thought to be one factor contributing to the 'dampening' effect on MOE in densified bamboo tissue, and this change likely has a small role in the relative reduction.

An additional explanation for the relative reduction of the densified materials' properties relates to differences in microfibril angle (MFA) between the inner and outer culm wall. A study by Wang et al. (2012) finds a substantially higher MFA in the inner region of the culm wall than that of the middle and outer region of the culm wall. This MFA difference could be related to the difference in properties of the densified (inner culm wall) and high density natural (outer culm wall) materials. However, other studies, which use a different definition of MFA, find little variation radially across the culm wall (Yu et al. 2007; Wang et al. 2010, 2014). This suggests the MFA difference found by Wang et al. (2012) may be related to the meso-scale changes in the tissue (i.e. the increase in fiber volume fraction across the culm wall) opposed to actual changes in the MFA of the fibers. Furthering this argument is the work of Wang et al. (2014), which suggests the mechanical properties of fibers from different positions in the culm vary little. The MFA explanation seems directly linked to the fiber volume fraction reasoning.

The reduced moduli and hardness values of the fibers, measured in the nanoindentation tests, are similar in both the natural and densified Moso material (**Table 1)**. Two-sample t-tests also show no statistically significant differences between the two groups' reduced modulus (p-value of 0.117) and hardness (p-value of 0.263) values. These nanoindentation results indicate that both the reduced modulus and hardness of the natural and densified fiber materials statistically have no significant difference, suggesting that the mechanical properties of the cell wall substance are unchanged by the VTC process. It is well known that thermal treatments generally decrease the mechanical properties of wood (Yildiz et al. 2006; Borrega and Kärenlampi 2008; Esteves and Pereira 2009). Studies that have found that the MOE and MOR of Moso bamboo decrease considerably after thermal treatments have used temperatures of 160˚C and above, for longer durations than the VTC process used in this study (Zhang et al. 2013). It is also noted that steam treatments at temperatures of 180ºC and 200ºC for as long as 8 minutes were found to reduce the bending properties of *Cryptomeria japonica* D. Don by less than 10% (Inoue et al. 1993). In the densification procedure of this study, the bamboo was only exposed to steam for roughly 2.5 min.

The models have significant limitations. Non-fiber cells of the vascular bundles are treated as the parenchyma; as noted, the volume fraction of such cells is likely small. The properties of the solid fiber, from literature values, extrapolated from tests on bamboo, are assumed not to change during densification; the present nanoindentation results support this assumption (**Table 1**). The parenchyma contributions to the mechanical properties are neglected entirely; the overall agreement between the models and mechanical data suggests this to be a reasonable assumption in all cases, but that of the densified bamboo's MOR. No lateral expansion is assumed in densification; as previously noted, Semple et al. (2013) report only

slight lateral expansion at a compression of 50%. Vascular bundle shape and distribution in the bamboo tissue is not considered in this treatment. Details regarding the parenchyma structure are similarly not taken into account. These assumptions cause breakdowns in the modelling of densification with natural tissue with high fiber volume fractions. A clear breakdown of the model occurs with natural tissue when the fiber volume fraction equals C (0.50 in this case). This tissue would densify to entirely fiber, which is clearly not possible. The model breaks down before this limit when the natural fiber volume fraction equals $\frac{\left(\rho^* / \rho_s\right)_p - C}{\left(\rho^* / \rho_s\right)_p - 1}$, which corresponds to the parenchyma's relative density increasing beyond 1 during densification. In this study, this limit occurs at a natural fiber volume fraction of roughly 0.36 corresponding to a natural material density of roughly 750 kg/m^3. The densification of higher density bamboo tissue cannot be modelled in this framework; however, densification of already high density tissue is of less interest. The rule of mixtures treatment of the MOR is not rigorous, as mentioned. Despite these many simplifications, the models satisfactorily reflect the density, longitudinal MOE, and longitudinal MOR of both the natural material and the densified material in this study.

Data for the MOE and MOR of Moso glulam and scrimber, with slightly higher moisture content (in the range of 6 to 8%) than the materials of this study, from four point bending tests from the work of Sharma and her colleagues are plotted in **Fig. 3** for comparison (Sharma et al. 2015a,b). The glulam beam dimensions were: width 60 mm, depth 120 mm and length 2400 mm; while the scrimber beam dimensions were: width 40 mm, depth 40 mm, length 800 mm.

The moisture content of the different groups of specimens shown in **Fig. 3** is not constant. The effect of adjusting the moisture content to a constant value on the MOE and MOR can be estimated from the effect of varying moisture content on the MOE and MOR of wood

(Bodig and Jayne 1982). The natural specimens tested in this study had a moisture content of 7%, the glulam specimens tested by Sharma et al. (2015a, b) had moisture content of 6-8% and the natural specimens tested previously had a moisture content of 4% (Dixon and Gibson 2014; Dixon et al. 2015). For an adjusted moisture content of 7%, the natural data of the previous study is estimated to increase in density by roughly 3% and to decrease in MOE and MOR by roughly 6% and 11%, respectively. The densified specimens tested in this study had a moisture content of 5%, while the scrimber specimens had a moisture content of 7% (Sharma et al. 2015a). For an adjusted moisture content of 7%, the density of the densified specimens is estimated to increase by roughly 2%, while the MOE and MOR would decrease by 4% and 8%. Adjusting for constant moisture content does not greatly change the data with respect to each other or the models.

Over the density range 640 to 690 kg/m^3, the glulam has MOE values between 10-12 GPa (Sharma et al. 2015a,b), similar to the natural bamboo and the model at this density range, as expected (**Fig. 3a**). In both the glulam and the natural material, the fiber volume fraction primarily governs the density and the longitudinal MOE; similar densities equate to similar fiber volume fractions (at similar moisture content), which in turn equate to similar MOE values. The substantially larger size of the Moso glulam should not affect the elastic response. However, the resin of the glulam complicates this comparison.

The modulus of rupture of the glulam and the natural bamboo are substantially different. The MOR of the glulam is roughly 80 MPa, over a density range of 640 to 690 kg/m^3 while that of the model for the natural material varies from roughly 125 to 145 MPa, giving an average knockdown factor 0.59. This difference is not unexpected; the Moso glulam specimens have a volume roughly four orders of magnitude larger than that of the flexural test specimens in this

study. Relating the glulam and the natural material by a size effect relationship would be over simplifying given the materials are two different systems with a high likelihood of different underlying failure mechanisms, though ultimate failure in both cases is at mid-span on the tensile side of the beams (and impractical given only two size-property data points and the relatively small sample size from which these points are constructed and the large variability in natural materials). However, it is worth noting that for this volume difference in wood glulam, strength knockdown factors of 0.36 (Douglas-fir and other species) and 0.60 (southern pines) are calculated with glulam size adjustment expressions (Smulski 1997). Similarly, the solid lumber MOR size effect expression for clear, straight-grained Douglas-fir gives a knockdown factor of 0.59 (Forest Products Laboratory 2010).

Both the MOE and MOR of Moso bamboo scrimber are lower than those of the densified Moso bamboo material. The scrimber MOE is 13 GPa, while that of the densified material at around the scrimber's density, 1163 kg/m^3, is generally 16 to 17 GPa. The scrimber MOR is 119 MPa, while that of the densified material ranges from 180 to 240 MPa (at around 1163 kg/m^3). The large scatter in the densified Moso material MOR limits the extent to which strength comparisons with scrimber can be considered. The reduction in both the MOE and MOR could be attributed to several factors. Bamboo scrimber is generally not densified in a way to avoid cell wall fracture, as is the case in the VTC densification of bamboo. This microstructural explanation is interesting and compelling, and warrants further exploration. However, differences in size (the scrimber specimens are roughly three orders of magnitude larger than the small densified specimens in volume), failure mechanisms, and more general differences in the systems (e.g. macrostructure) are hypothesized to have a larger role in the reduction.

The bending stiffness performance index, which minimizes the mass of a beam of a given stiffness, is given by $\sqrt{E}/\rho$ (Ashby 2000). Similarly, the bending strength performance index, which minimizes the mass of a beam of given strength, is given by $MOR^{2/3}/\rho$ (Ashby 2000). The ranges of these quantities for the natural and densified material of this study, as well as average values for the glulam and scrimber, are given in **Table 2**. The densified material's ranges are lower than those of the natural material. In the case of $\sqrt{E}/\rho$, the glulam and scrimber values fall into the ranges of their roughly-equivalent materials, the natural and VTC densified bamboo, respectively. For $MOR^{2/3}/\rho$, both materials fall just outside their respective counterparts' ranges. It should be noted that the performance indices vary with density, so they do not represent intrinsic material characteristics. To address this, the models have been used to estimate the performance indices at the glulam and scrimber densities for the natural and densified material, respectively. The performance index comparisons, together with the previous direct comparison of properties at a given density, give a sense for the similarities and differences between the materials.

Conclusion

Moso bamboo densification increases the flexural properties along the longitudinal direction of the material. However, the properties of the natural material are higher than those of the densified material at similar densities. This is primarily due to the structure of the bamboo. The dense fibers, which dominate longitudinal properties, probably experienced no significant densification in this study. During densification, the parenchyma densifies and vessels close, increasing the fiber volume fraction within the tissue, but not to an extent such that the densified bamboo's MOE and MOR reach those of the natural material at the same density. The simple

models of the densification and the densified flexural properties further suggest this to be the case. A number of aspects of bamboo densification need to be considered with a more advanced model: the geometry and density variation of the fibers is certainly one, as is the distribution, shape and flattening of the vascular bundles and the geometry of the parenchyma. A deep understanding of transverse cell wall properties (fiber and parenchyma properties and their dependence on temperature and moisture content) would have to be combined with these details of the bamboo structure for a truly complete model of densification. Moso glulam and scrimber are bamboo products somewhat analogous to the natural and THM densified Moso tissue, respectively. In this work, flexural properties are only compared simply and put into the same context. Further work is recommended to understand size effects in bamboo and bamboo products, relate clear bamboo tissue properties with bamboo glulam properties, and determine optimum densification levels for bamboo.

Acknowledgements

This paper is based upon work supported by the National Science Foundation under OISE: 1258574. The views expressed in this paper are not endorsed by the National Science Foundation. Research at UBC on densification of bamboo was supported by the National Science and Engineering Research Council of Canada (NSERC), and the Green Building Materials Laboratory at Oregon State University (OSU). We would like to thank Alan Schwartzman for training and assistance with the Hysitron TriboIndenter.

References

Amada S, Ichikawa Y, Munekata T, Nagase Y, Shimizu H (1997) Fiber texture and mechanical graded structure of bamboo. Compos Part B Eng 28B:13–20.

Archila-Santos HF, Ansell MP, Walker P (2014) Elastic properties of thermo-hydro-mechanically modified bamboo (Guadua angustifolia Kunth) measured in tension. Key Eng Mater 600:111–120.

Ashby MF (2000) Multi-objective optimization in material design and selection. Acta Mater 48:359–369.

Bodig J, Jayne BA (1982) Mechanics of Wood and Wood Composites. Van Nostrand Reinhold, New York

Borrega M, Kärenlampi PP (2008) Mechanical behavior of heat-treated spruce (Picea abies) wood at constant moisture content and ambient humidity. Holz Roh- Werkst 66:63–69.

Dixon PG, Ahvenainen P, Aijazi AN, et al (2015) Comparison of the structure and flexural properties of Moso, Guadua and Tre Gai bamboo. Constr Build Mater 90:11–17.

Dixon PG, Gibson LJ (2014) The structure and mechanics of Moso bamboo material. J R Soc Interface 11:20140321–20140321.

Esteves BM, Pereira HM (2009) Wood modification by thermal treatment: a review. BioResources 4:370–404.

FAO (2010) Global Forest Resources Assessment 2010. Food and Agriculture Organization of the United Nations (FAO), Rome

Forest Products Laboratory (2010) Wood Handbook. Forest Products Laboratory USDA, Madison, Wisconsin

Gibson LJ, Ashby MF (1997) Cellular Solids: Structure and Properties, 2nd edn. Cambridge University Press, Cambridge, UK

Gritsch CS (2004) Developmental Changes in Cell Wall Structure of Phloem Fibres of the Bamboo Dendrocalamus asper. Ann Bot 94:497–505.

Grosser D, Liese W (1971) On the anatomy of Asian bamboos, with special reference to their vascular bundles. Wood Sci Technol 5:290–312.

Inoue M, Norimoto M, Tanahashi M, Rowell RM (1993) Steam or heat fixation of compressed wood. Wood Fiber Sci 25:224–235.

Jiang Z (2007) Bamboo and Rattan in the World. China Forestry Publishing House, Beijing, China

Kamke FA (2006) Densified radiata pine for structural composites. Maderas Cienc Tecnol 8:83–92.

Kamke FA, Casey LJ (1988) Fundamentals of flakeboard manufacture: internal-mat conditions. For Prod J 38:38–44.

Kamke FA, Rathi VM (2011) Apparatus for viscoelastic thermal compression of wood. Eur J Wood Wood Prod 69:483–487.

Kamke FA, Sizemore H (2008) Viscoelastic thermal compression of wood. US Patent No. 7404422.

Kutnar A, Kamke FA, Sernek M (2008) The mechanical properties of densified VTC wood relevant for structural composites. Holz Roh- Werkst 66:439–446.

Kutnar A, Kamke FA, Sernek M (2009) Density profile and morphology of viscoelastic thermal compressed wood. Wood Sci Technol 43:57–68.

Lam F (2001) Modern structural wood products. Prog Struct Eng Mater 3:238–245.

Lee AWC, Bai X, Peralta PN (1996) Physical and mechanical properties of strandboard made from moso bamboo. For Prod J 46:84–88.

Liese W (1987) Research on bamboo. Wood Sci Technol 21:189–209.

Liese W, Weiner G (1996) Ageing of bamboo culms. A review. Wood Sci Technol 30:77–89.

Liu H, Jiang Z, Zhang X, Liu X, Sun Z (2014) Effect of fiber on tensile properties of moso bamboo. BioResources 9:6888–6898.

Lo TY, Cui H, Leung H (2004) The effect of fiber density on strength capacity of bamboo. Mater Lett 58:2595–2598.

Lugt P van der (2008) Design interventions for stimulating bamboo commercialization: Dutch design meets bamboo as a replicable model. Doctoral, VSSD

Ramage M, Sharma B, Bock M, et al (2015) Engineered bamboo: state of the art. Proc ICE - Constr Mater 168:57–67.

Semple KE, Kamke FA, Kutnar A, Smith GD (2013) Exploratory thermal-hydro-mechanical modification (THM) of moso bamboo (Phyllostachys pubescens Mazel). In: Characterisation of Modified Wood in Relation to Wood Bonding and Coating Performance. eds S. Medved and A. Kutnar, Rogla, Slovenia, pp 220–227

Semple KE, Vnučec D, Kutnar A, et al (2015a) Bonding of THM modified Moso bamboo (Phyllostachys pubescens Mazel) using modified soybean protein isolate (SPI) based adhesives. Eur J Wood Wood Prod 73:781-792.

Semple KE, Zhang PK, Smith GD (2015b) Hybrid oriented strand boards made from Moso bamboo (Phyllostachys pubescens Mazel) and Aspen (Populus tremuloides Michx.): species-separated three-layer boards. Eur J Wood Wood Prod 73:527-536.

Semple KE, Zhang PK, Smith GD (2015c) Stranding moso and guadua bamboo. Part I. Strand production and size classification. BioResources 10:4048–4064.

Semple KE, Zhang PK, Smith GD (2015d) Stranding moso and guadua bamboo. Part II. Strand surface roughness and classification. BioResources 10:4599–4612.

Shao Z-P, Fang C-H, Huang S-X, Tian G-L (2010) Tensile properties of Moso bamboo (Phyllostachys pubescens) and its components with respect to its fiber-reinforced composite structure. Wood Sci Technol 44:655–666.

Sharma B, Gatóo A, Bock M, Ramage M (2015a) Engineered bamboo for structural applications. Constr Build Mater 81:66–73.

Sharma B, Gatóo A, Ramage MH (2015b) Effect of processing methods on the mechanical properties of engineered bamboo. Constr Build Mater 83:95–101.

Shaw MC, Sata T (1966) The plastic behavior of cellular materials. Int J Mech Sci 8:469–478.

Smulski S (1997) Engineered Wood Products: A guide for specifiers, designers and users. PFS Research Foundation, Madison, Wisconsin

Sumardi I, Ono K, Suzuki S (2007) Effect of board density and layer structure on the mechanical properties of bamboo oriented strandboard. J Wood Sci 53:510–515.

Sumardi I, Suzuki S, Rahmawati N (2015) Effect of Board Type on Some Properties of Bamboo Strandboard. J Math Fundam Sci 47:51–59.

Vogtländer J, van der Lugt P, Brezet H (2010) The sustainability of bamboo products for local and Western European applications. LCAs and land-use. J Clean Prod 18:1260–1269.

Wang H, An X, Li W, Wang H, Yu Y (2014) Variation of mechanical properties of single bamboo fibers (Dendrocalamus latiflorus Munro) with respect to age and location in culms. Holzforschung.

Wang XQ, Li XZ, Ren HQ (2010) Variation of microfibril angle and density in moso bamboo (Phyllostachys pubescens). J Trop For Sci 22:88–96.

Wang Y, Leppänen K, Andersson S, Serimaa R, Ren H, Fei B (2012) Studies on the nanostructure of the cell wall of bamboo using X-ray scattering. Wood Sci Technol 46:317–332.

Winistorfer PM, Moschler WW, Wang S, DePaula E, Bledsoe BL (2000) Fundamentals of vertical density profile formation in wood composites. Part I. In-situ density measurement of the consolidation process. Wood Fiber Sci 32:209–219.

Wolcott MP, Kamke FA, Dillard DA (1994) Fundamental aspects of wood deformation pertaining to manufacture of wood-based composites. Wood Fiber Sci 26:496–511.

Yildiz S, Gezer ED, Yildiz UC (2006) Mechanical and chemical behavior of spruce wood modified by heat. Build Environ 41:1762–1766.

Yu Y, Fei B, Zhang B, Yu X (2007) Cell-wall mechanical properties of bamboo investigated by in-situ imaging nanoindentation. Wood Fiber Sci 39:527–535.

Yu Y, Zhu R, Wu B, Hu Y, Yu W (2015) Fabrication, material properties, and application of bamboo scrimber. Wood Sci Technol 49:83–98. doi: 10.1007/s00226-014-0683-7

Zhang YM, Yu YL, Yu WJ (2013) Effect of thermal treatment on the physical and mechanical properties of phyllostachys pubescen bamboo. Eur J Wood Wood Prod 71:61–67.

Tables

Table 1 – Nanoindentation results

	Reduced Modulus [GPa]	**Hardness [MPa]**
Natural	15.7 ± 2.2	341 ± 78
Densified	16.1 ± 1.5	330 ± 58

Values are mean ± standard deviation

Table 2 – Flexural performance indices

	$\sqrt{E}/\rho$ **[GPa$^{1/2}$ m^3/kg]**	$MOR^{2/3}/\rho$ **[MPa$^{2/3}$ m^3/kg]**
Natural	0.0035 - 0.0058	0.029 - 0.045
VTC Densified	0.0029 - 0.0040	0.022 - 0.037
Glulam	0.0049	0.028
Scrimber	0.0031	0.021
Natural model (ρ = 668 kg/m^3)	0.0051	0.040
Densified model (ρ = 1163 kg/m^3)	0.0036	0.030

List of Figures

Figure 1 – Strip and flexural specimen orientation, entire strips shown with dashed lines, beams with solid lines

Figure 2 – Low vacuum secondary mode SEM micrographs of Moso bamboo (uncoated). (a): Natural undensified cross-section; (b): densified; cross-section

Figure 3 – (a) Longitudinal MOE and (b) longitudinal MOR plotted against density from bending tests

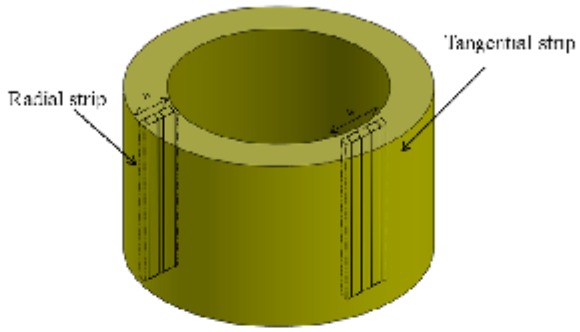

Figure 1 – Strip and flexural specimen orientation, entire strips shown with dashed lines, beams with solid lines, "w" refers to strip width

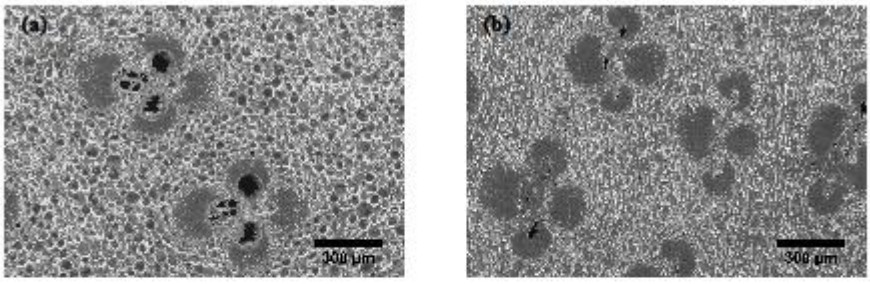

Figure 2 – Low vacuum secondary mode SEM micrographs of Moso bamboo (uncoated). **(a)**: Natural undensified cross-section; **(b)**: Densified cross-section.

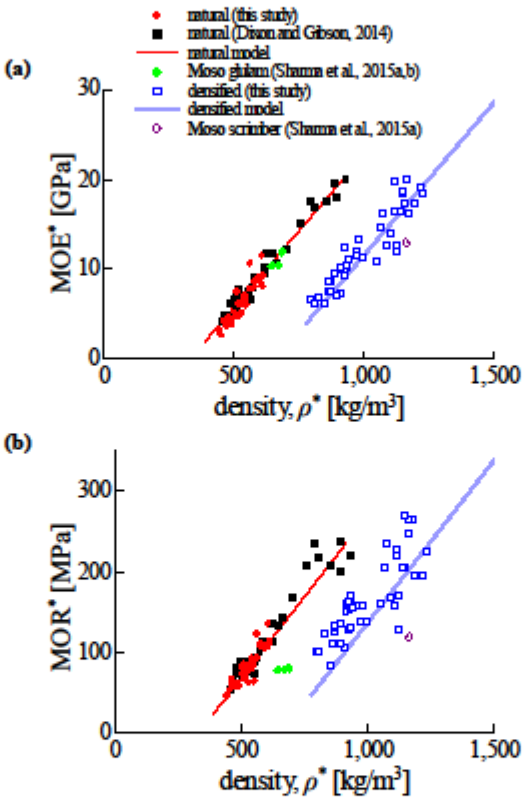

Figure 3 – (a) Longitudinal MOE and (b) longitudinal MOR plotted against density from bending tests